Pramāṇa, Vol. 4, No. 5, 1975, pp 229-241. © Printed in India

Characteristics of a high frequency ion source used in a low-energy accelerator

MOHAMED E ABDELAZIZ*, MOHAMED A EID† and FATMA ABDELSALAM**

* Physics Department, Faculty of Science, University of Tripoli, Libya.
† Physics Department, Faculty of Education, University of Tripoli, Libya.
** Accelerator Department, Egyptian Atomic Energy Establishment, Cairo, Egypt.

MS received 8 July 1974; after revision 31 January 1975.

Abstract. This work presents the characteristics of a high frequency ion source operating on a low energy, 150 keV accelerator. The latter is to be used as a neutron generator and its design is based on a theoretical analysis which shows that if the axial potential in an electrostatic electrode system is made to increase with four thirds the power of axial distance, inward electric forces will compensate space charge forces tending to blow up the beam. This results in a simplified acceleration tube much shorter and of higher gradient than the conventional acceleration columns. The ion source itself is an ordinary type using axial extraction of the beam, and its main properties investigated are the beam current and beam quality (or emittance). Dependence of the two on different parameters is investigated in a series of tests.

Keywords. Neutron generator; high frequency ion source; low energy accelerator.

1. Introduction

Although extensive work has been carried out on various types of intense ion sources*, the radio frequency source still maintains its known advantages of high efficiency with respect to gas consumption, simplicity of construction, low cost, high proton percentage, as well as long and trouble-free operation. The r.f. source tested in this work uses axial extraction of its beam in the direction of the r.f. field. The design of such sources has usually been a matter of trial and error. But in this work, the ion source design and analysis is based on two principles: first is that the ionization density should be as high as possible with the maximum proton percentage; the second is the efficient extraction and best focusing of the beam into the exit canal of the source. One has, therefore, to consider optimum conditions for the creation of an intense plasma on the one hand, and study carefully the geometry of the extraction electrode for the emission of positive ions from the plasma boundary and subsequent focussing of them into a collimated beam into the exit canal on the other. This together with a suitable size of the exit canal to maintain proper gas pressure in the source and a good vacuum in the acceleration tube would lead to an efficient ion source both with respect to gas consumption and to absorbed r.f. power.

* *See Proceedings of First International Conference on Ion Sources*, Saclay, France, 1969.

A beam with good phase properties after extraction from the source will be handled efficiently when injected into and accelerated by the acceleration column. We use a short three-electrode system which serves to accelerate as well as to focus the positive ion beam and which can create a high gradient field with no magnetic lens. Thus, we get an acceleration column much shorter than the conventional types. In this device the axial potential along the acceleration column is made to increase with 4/3 the power of axial distance which results in inward radial electric forces that compensate space charge forces tending to blow up the beam.

Measurement of the extracted ion beam deals with two main properties: (*a*) the beam current and its dependance on the acceleration voltage and parameters, (*b*) the beam emittance represented by area of phase-space diagram, *i.e.*, the diagram obtained by plotting angle of beam divergence α *versus* beam radius r for beam positions admitted through a small aperture and received downstream on a multi-channel strip collector. This also gives current density distribution in phase-space, and beam brightness.

Although our tests were performed at low acceleration voltages, results show that the use of the short acceleration column delivers a beam with favourable properties, and will naturally still give better beam quality at higher voltages.

2. Apparatus theory and description

The low energy accelerator used in these tests is shown in figure 1. It consists

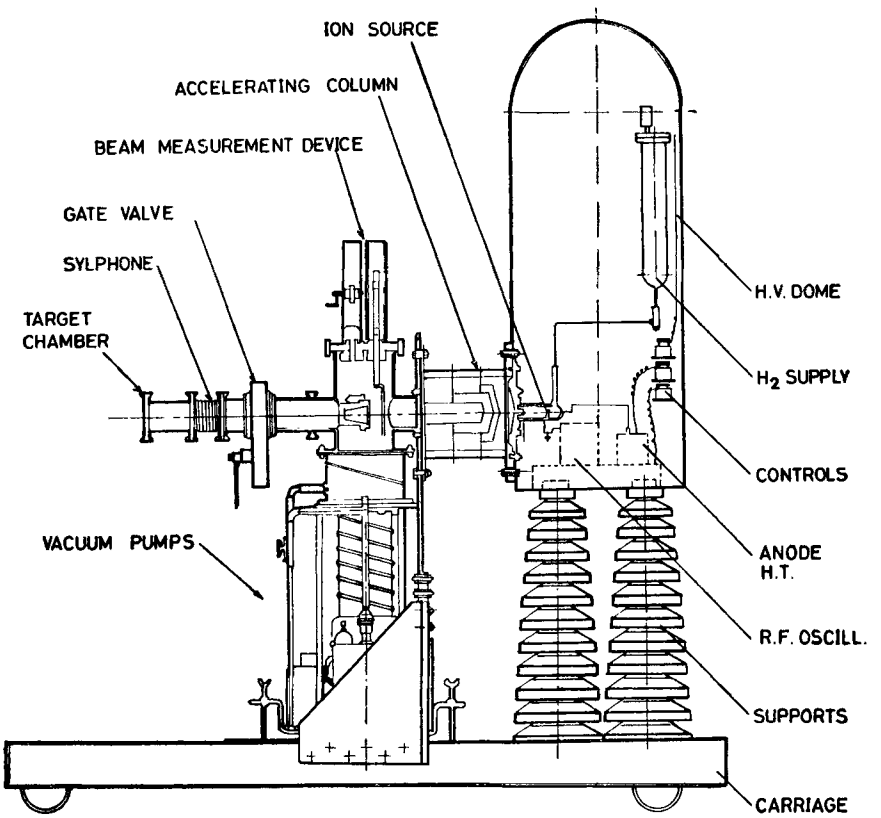

Figure 1. Schematic arrangement of the 150-keV accelerator.

basically of: the ion source together with its high frequency (50 Mc). Colpitts oscillator, 10 kV extraction supply, and gas supply, all enclosed in a 150 kV platform and dome supported on high voltage insulators. The ion source flange is fixed to the three-electrode acceleration column supported on the ground plate, then comes the beam measuring device consisting of the Faraday cup for beam current measurements, and the device for beam quality detection. The latter uses a multi-channel collector with 10 strips, each of them 0·2 mm wide, and an upstream narrow slit with 12 cm axial separation. These measuring devices are controlled by servomechanisms fixed over the vacuum line which carries a gate valve to isolate the vacuum system from the target. Since the high voltage for acceleration is applied to the dome, the low tension 220 V which feeds the circuits inside the dome is applied through an isolation transformer insulated for high voltage and having a turns ratio of 1 : 1.

2.1. *The ion source*

In order to produce an intense r.f. plasma, one has to achieve proper matching between the oscillator and the load represented by the source's plasma. The radial density distribution follows a Bessel function of the zero order (Abdelaziz 1962).

$$n_r = n_0 . J_0\left(r \sqrt{\frac{\gamma}{k}}\right) \tag{1}$$

where n_0 is the electron density at the tube axis, and γ the number of electrons produced per second by each electron mainly due to secondary emission from the tube walls. This is because at such low pressures where the mean free path is large compared to the tube dimensions collisions of electrons oscillating in the r.f. field are more probable than collisions with gas molecules. K in eq. (1) is the diffusion coefficient, and since the density drops to zero at the tube radius R, it is easy to see that

$$n_r = n_0 J_0 \frac{(2{\cdot}405\, r)}{R} \tag{2}$$

In addition to the density being maximum at the tube axis, one would also expect that beam extraction is preferable at points inside the source's plasma and remote from the tube walls which are surfaces of recombination of atomic to molecular ions. Furthermore, the use of wall material like pyrex which has the smallest recombination coefficient, and the reduction to minimum of metallic surfaces would all co-operate to give maximum current and high proton percentage reaching more than 90%. On the other hand, having achieved high ion density, the next problem would be that of beam extraction. The design of the extraction electrode falls into two stages:

(i) consideration of the exit canal size for maximum current transmission and for gas flow which creates the suitable pressure difference between the source and the high vacuum region. Thus, if we consider a beam of circular symmetry about the Z axis (figure 2), it could be shown (Abdelaziz 1960) that the beam spread curve for protons will be given by,

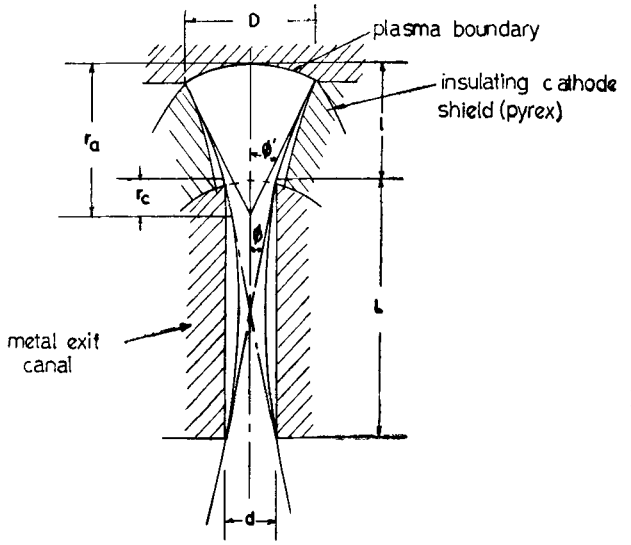

Figure 2. Beam profile in the extraction electrode.

$$\frac{Z}{r_0} = \frac{1}{0{\cdot}201} \cdot \frac{V_{(\mathrm{kV})}^{\frac{3}{4}}}{I_{(\mathrm{mA})}^{\frac{1}{2}}} \int_1^{r/r_0} \frac{d(r/r_0)}{\sqrt{\log (r/r_0)}} \tag{3}$$

where r_0 is the minimum beam radius (beam waist) at canal centre, and I the beam current whose maximum value could be shown to be given by,

$$I_{\max} = 28{\cdot}8\, V_{(\mathrm{kV})}^{3/2} \cdot \left(\frac{d}{L}\right)^2 \qquad \mathrm{mA} \tag{4}$$

d being canal diameter and L its length.

On the other hand, considering molecular flow F in the canal at room temperature, we get,

$$F = \frac{111\pi d^2}{1 + 0{\cdot}75\,\frac{L}{d}}\ \mathrm{cm^3/sec.}$$

where d and L are in mm.

Now, for a gas pressure p microns in the source, the gas consumption G referred to atmospheric pressure will be,

$$G = \frac{1{\cdot}655\, d^2 p}{1 + 0{\cdot}75\,\frac{L}{d}}\ \mathrm{cm^3/hr} \tag{5}$$

From eqs 4 and 5 we get,

$$I_{\max} = \frac{16{\cdot}2\, V_{(\mathrm{kv})}}{\left[\frac{1{\cdot}655 d^2 p}{G} - 1\right]^2} \qquad \mathrm{mA} \tag{6}$$

which gives the maximum extracted beam current as a function of extraction potential, canal diameter, gas consumption and pressure. If we plot $I_{\max}$ as a function of canal radius ($d/2$) for a given gas consumption and for a value of the pressure normally used, with extraction voltage as parameter, we get what may be

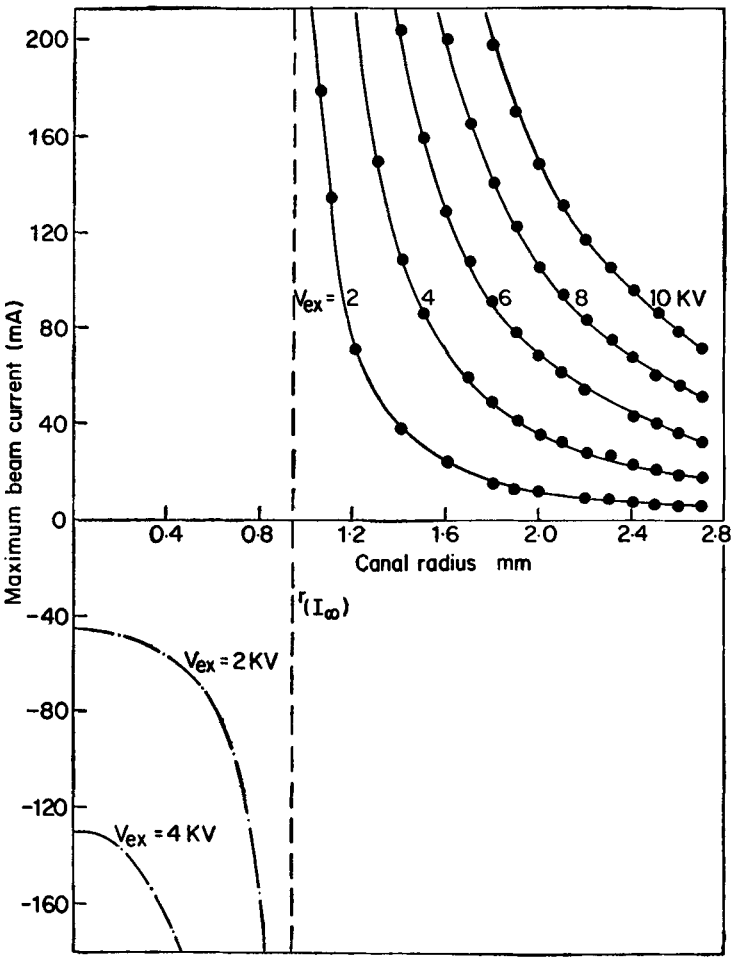

Figure 3. Canal design chart for constant gas consumption (G = 30 cc/hr, P = 5 μ).

called the constant-gas-consumption chart for exit canal design, as shown in figure 3. The canal length as obtained from eq. (5) is given by,

$$L_{mm} = 1{\cdot}33\, d \left[\frac{1{\cdot}655\, d^2 p}{G} - 1\right] \tag{7}$$

The curves in the design chart vary in an interesting manner: it is seen from figure 4 and eq. (7) that as the canal diameter d is reduced the length will also have to be reduced in order to keep the pressure and gas consumption constant, until at a point where $L = 0$, the ion current from eq. (6) and figure 3 is theoretically infinite (or practically maximum as the ion current is naturally limited by the plasma density).

(ii) The second step would be the focussing of the beam—as specified by the above conditions—as it is emitted from the plasma boundry to enter the exit canal following the beam profile indicated in figure 2. This means that the insulating cathode shield above the exit canal is designed by equating its *perveance* to that of the canal. The conical part of the convergent beam above the exit canal is regarded as being analogous to the electron beam of a high efficiency Pierce electron

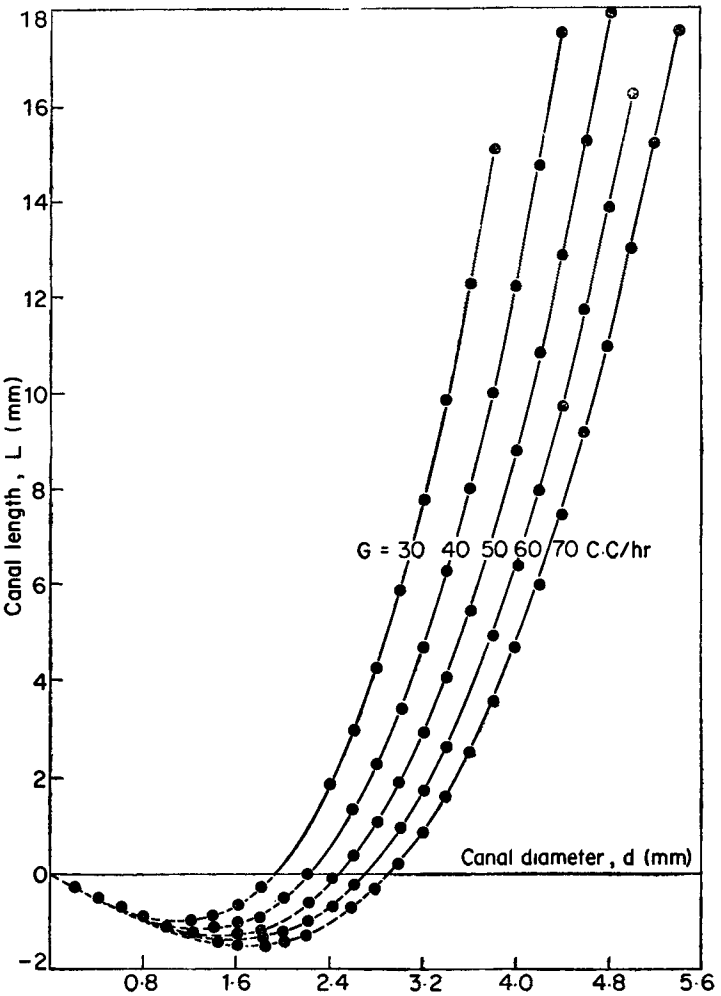

Figure 4. Variation of canal length with its diameter for constant gas consumption.

gun (Pierce 1940). The radial current flow in a cone of semi angle θ' (figure 2) cut out of a sphere of radius r_a can be shown (Abdelaziz 1960) to be given by,

$$I = 0{\cdot}688 \times 10^{-6} V_{(\text{Volt})}^{3/2} \frac{\sin \frac{\theta'}{2}}{\alpha^2} \quad \text{A} \tag{8}$$

Where V is the anode (extraction) voltage, and α^2 a function of r_a/r_0, and is given by tables (Langmuir and Blodgett 1923). Accordingly, it is easy to show that,

$$\sin \theta' = \frac{1{\cdot}048 \times 10^3 \sqrt{I/V^{\frac{3}{4}}}}{1 - \frac{1}{6\alpha^2} r_a/r_c \left| \frac{d(\alpha^2)}{d(r_a/r_c)} \right| r_c} \tag{9}$$

where

$$\tan \theta = \frac{d}{L} \text{ (figure 2)}$$

From this analysis, and the simple geometry of the cathode, the diameter D of the cathode shield and its height l above the canal could be calculated. Table 1 gives calculation results for a complete design of the extraction system corresponding to a canal length = 10 mm. The result is the source shown in figure 5. The arrangement of extraction canal is shown in figure 6.

Table 1. Calculation results for the extraction geometry (dimensions in mm), for $L = 10$ mm.

d	P (X10^{-8}) $\frac{\text{amp}}{\text{Volt}^{3/2}}$	θ'(°)	D	r_a	l
2·0	3·664	26·30	4·30	4·85	2·56
2·5	5·725	32·80	5·38	4·97	2·66
3·0	8·244	39·50	6·45	5·08	2·72
3·5	11·221	46·00	7·53	5·24	2·81
4·0	14·656	52·40	8·60	5·43	2·91
4·5	18·549	59·00	9·68	5·65	3·03
5·0	22·90	65·70	10·75	5·90	3·16

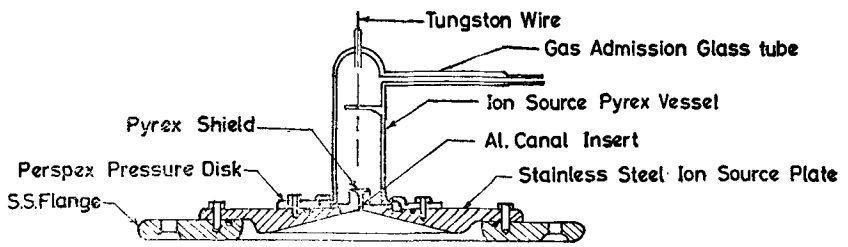

Figure 5. Ion source assembly.

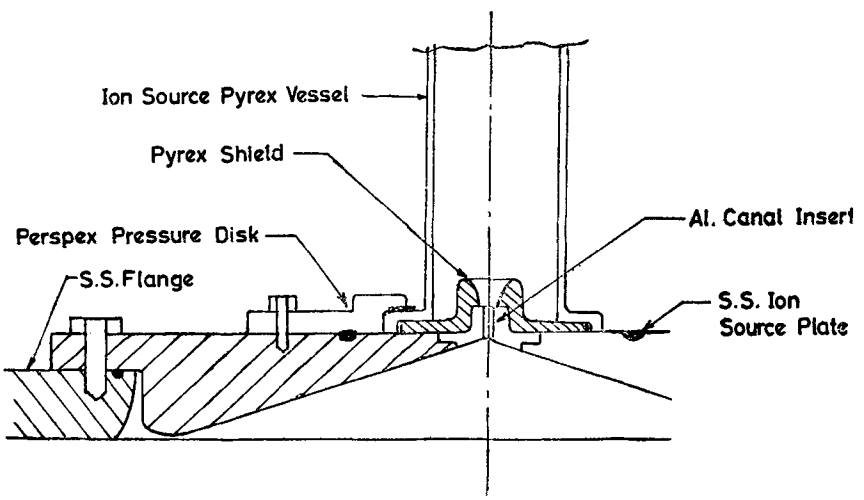

Figure 6. Extraction electrode of the ion source.

2.2. *The high gradient acceleration column*

The theory of the acceleration column has been described elsewhere (Abdelaziz and Elnahas 1969). It results in the design of a short three-electrode device (figure 1). The basic idea is that if the axial potential is made to increase with the 4/3 power of axial distance, inward electric forces will compensate space charge forces tending to blow up the beam. A series of accelerating electrodes which conform to certain pre-calculated shapes yield a $Z^{4/3}$ potential distribution in each gap such that the beam is suitably confined and gradients of reasonable magnitudes are produced. The equation used for calculating the electrode shapes for the electrolytic tank model is,

$$\rho = \pm 3Z \cdot \left\{1 + \frac{V}{AZ^{4/3}}\right\}^{\frac{1}{2}} \tag{10}$$

where ρ is the radial distance from the axis, and V the acceleration potential, such that for any axial distance Z there will be an equipotential surface $V = -AZ^{4/3}$, where A is a constant. On the other hand, for numerical computation using electrolytic tank data, we use a modified form of the beam trajectory equation,

$$R'' + \frac{3}{16} R \frac{(V')^2}{(V)} - \frac{I}{4\pi\epsilon_0 \left(\frac{2e}{m}\right)^{\frac{1}{2}} VR} = 0 \tag{11}$$

where ϵ_0 is the permittivity of free space, e the electronic charge and m its mass, V' and R'' are the first and second derivatives with respect to Z. In eq. 11, a change of variables $\rho = RV^{\frac{1}{4}}$ has been made. Results of numerical integration of this equation show that the beam becomes nearly parallel at a radius of 1·7 mm when $Z = 6{\cdot}26$ mm and $V = 330$ kV, the initial radius being 1 mm.

2.3. *The beam measuring device*

First, the current is measured in a Faraday cup collector provided with a negative grid bias to eliminate error due to secondary electron emission from the cup. The beam emittance measurement, however, requires a more complicated system. We have first to understand what is meant by beam quality or emittance; this is the area of phase space obtained from the plot of P_r *versus* r, where P_r is radial momentum at radius r of the beam. But $P_r = mv_r = (2\ \text{emV})^{\frac{1}{2}}$. $dr/dz = \text{const.}\ dr/dz$, *i.e.*, proportional to α, angle of beam divergence.

Plots of α and r are obtained by allowing very small portions of the beam admitted through a narrow upstream slit to diverge over an axial distance Z at which a multi-channel strip electrode collector (figure 7) detects current signals to give both beam divergence and density distribution. The total strip electrode width is 16 mm and consists of 10 strips, each 0·2 mm thick. Thus, for each radial distance r of the slit, the beam profile is obtained both in the X and Y scans of the beam. Plots of α-r curves give:

Normalized beam emittance $E_n = A\beta\gamma/\pi$ (mm milliradian), and beam brightness.

$$B_n = \frac{2I \cdot 10^6}{\pi E_n^{\,2}}\ (\text{mA/mm.}^2\ \text{rad.}^2),$$

where A is the area of emittance diagram in mm milliradian, I the beam current in mA, $\beta = V/C$, $\gamma = (1 - \beta^2)^{\frac{1}{2}}$, V being particle velocity, and C the velocity of light.

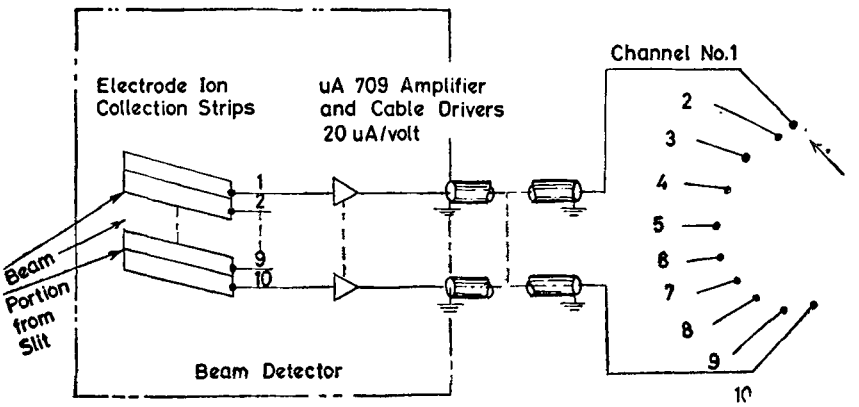

Figure 7 *a*. Strip electrode arrangement for beam analysis and emittance.

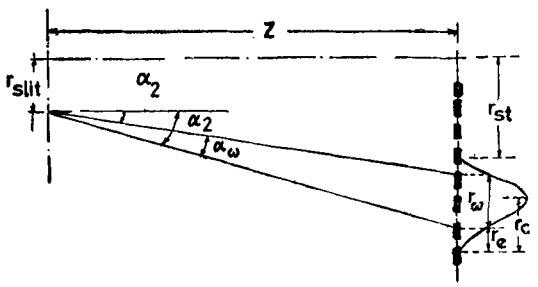

Figure 7 *b*. Estimation of beam density distribution.

3. Results and comments

After the source has been thoroughly cleaned and normalized, and the pressure in the system is brought down to 10^{-6} mm Hg, the following results are obtained.

3.1. *Extraction characteristics of the source*

The extracted ion current is measured with variation of anode extraction potential, the r.f. power being constant and gas pressure equal to about 5 μ. The test is repeated with a variation of the cathode-shield height above the exit canal ($l = 2$, 3 and 5 mm). It is seen (figure 8) that the beam current increases with the extraction voltage according to the Langmuir 3/2 – law. It is obvious that at higher extraction voltages, the beam focussing into the exit canal becomes more favourable as l is reduced. This also implies that optimum conditions for plasma boundary formation correspond to higher values of V_{ex} and lower values of l. The effect of gas pressure on the extracted beam current is seen from figure 9 for constant values of r.f. power and for $V_{ex} = 3$ kV, indicating a peak at a pressure as low as 0·4 μ. This shows that there exists a pressure that corresponds to an optimum mean free path at which the overall cross-section for excitation and ionization of gas particles is maximum. The current obtained at this low pressure is more than 500 μA which means that the source's efficiency with respect to gas consumption is fairly high. Furthermore, operation at such a low pressure adds the advantage

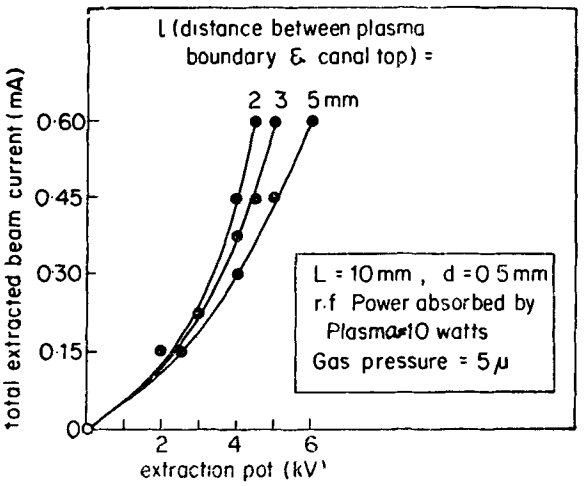

Figure 8. Variation of ion beam current with extraction voltage for different values of spacing above canal top.

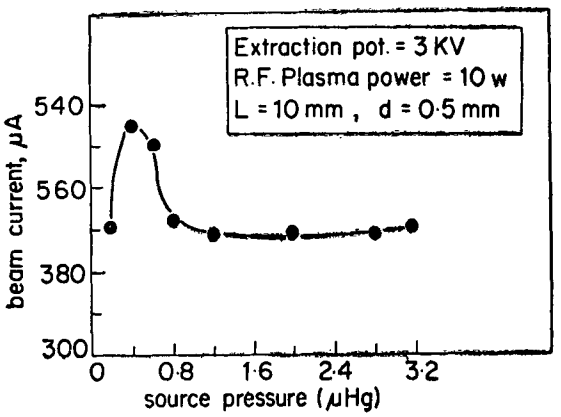

Figure 9. Variation of beam current with gas pressure in the source.

that high degree of vacuum in the acceleration tube eliminates losses of beam particles due to collisions with gas molecules, and avoids high voltage breakdown at values greater than 150 kV. It must be noted that operation below $0{\cdot}1\,\mu$ is very unstable because of the difficult and intermittent initiation of the source's plasma.

In a test showing the variation of beam current with acceleration voltage, it is seen (figure 10) that the current increases continuously with voltage; first at a high rate confirming that electrostatic focussing causes beam collimation and collection of more particles which are lost to the acceleration electrodes before acceleration. The rate of current increase is then reduced and we approach the 4/3 condition of acceleration.

3.2. *Phase-space characteristics*

The density distribution from which angular spread of the beam is detected has been measured for two cases, with and without acceleration. For the first case the acceleration voltage = 30 kV and we get the radial density distribution curve shown in figure 11, which is repeated for different radii of the beam as indicated by the position of the upstream slit. Then the $\alpha - r$ plot (figure 12) gives the emittance diagram fron which we get: emittance area $A = 113$ mm milliradian,

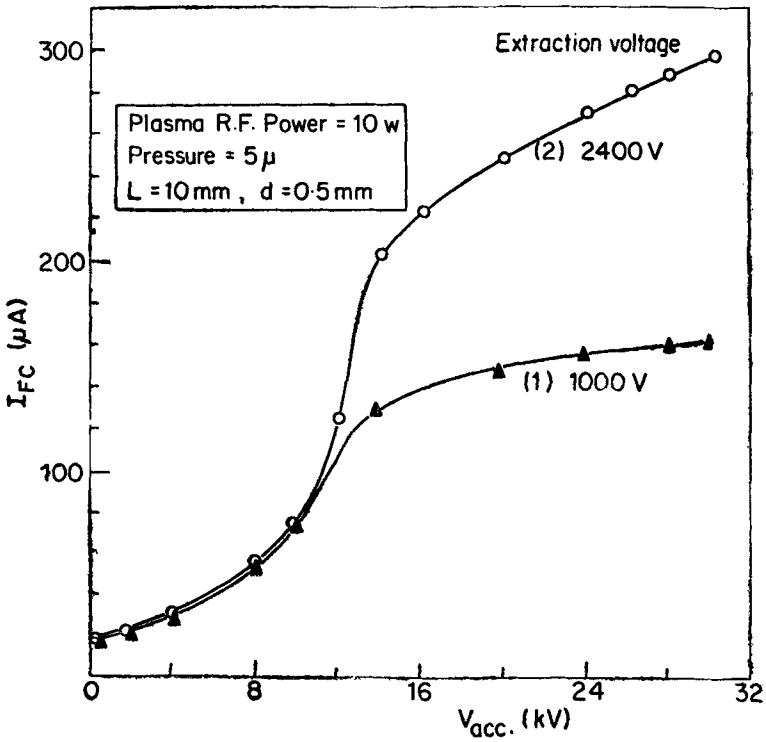

Figure 10. Variation of collected beam current with acceleration voltage.

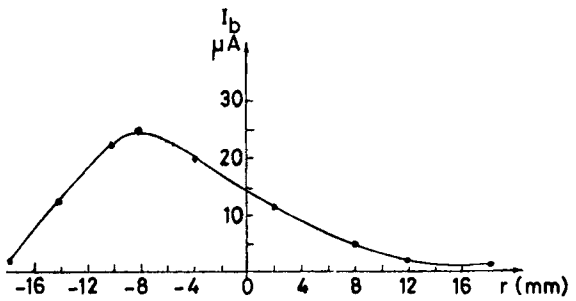

Figure 11. Beam density distribution of the accelerated beam ($V_{acc} = 30$ kv).

such that the normalized emittance $E_2^n = 7 \cdot 14$ mm milliradian, and beam brightness $B_n = 0 \cdot 64$ mA/cm^2. radian^2. In the second case, with no acceleration, we get the density distribution curve (figure 13) and the emittance diagram (figure 14), where $A = 59 \cdot 3$ mm milliradian, $E_n = 3 \cdot 7$ mm milliradian, and $B_n = 0 \cdot 8$ mA/cm^2. radian^2. Let us first consider the shape of the emittance figure. Ideally, this is supposed to be an ellipse whose shape shows whether the beam is convergent, divergent or parallel. Our results, however, yield ellipses with some distortion and with a slope showing that the beam is divergent. The divergence is due to small or no acceleration, while the distortion seems to be due to irregularities in the plasma boundary shape with the source and non-uniformity of beam density.

On the other hand, the reason that emittance is higher and brightness is lower

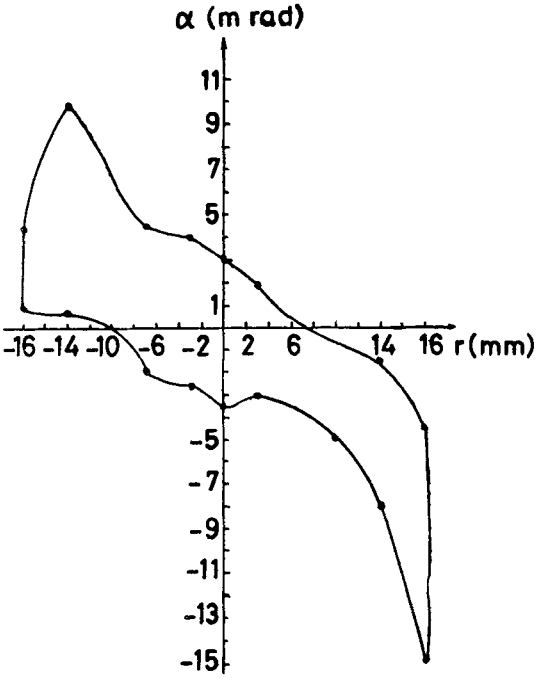

Figure 12. Beam emittance diagram of the accelerated beam (corresponding to figure 11).

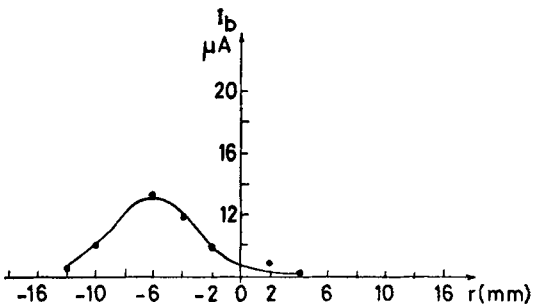

Figure 13. Beam density distribution of the ion source beam (without acceleration).

with the 30 kV rather than with no V_{acc} is that when the beam is accelerated it becomes less divergent and more intense as seen from the beam profile curves. However, the comparison here is not accurate since with no acceleration large portions of the beam are lost to the acceleration electrodes. It is, therefore, essential that the acceleration voltage be increased to such high values as to be able to accumulate the current to its saturated value and yet be capable of maintaining sufficiently high gradients to satisfy the 4/3 condition explained previously. When the beam current increases at such low energy (30 keV) space charge blow-up forces are set up causing higher emittance. It is also noticed that the more the beam current, the more distorted the emittance figure.

4. Conclusions

or the case of a low energy accelerator to be used as a neutron generator where

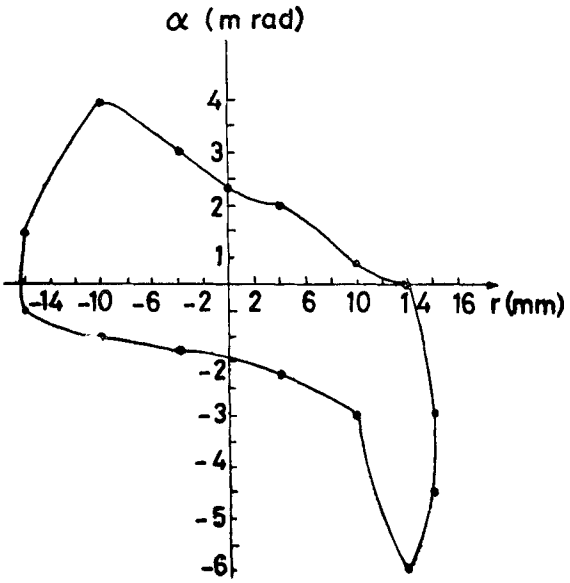

Figure 14. Beam emittance diagram of the ion source beam of figure 13.

the current is required to be of low value in the range of a few hundred micro-amperes, the r.f. ion source seems to be excellent. A reasonably high current at a low gas consumption features its beam. The extraction characteristics are favourable, and beam quality is satisfactory. On the other hand, the use of the short acceleration column proves to be successful in furnishing relatively high electric gradients and in providing a beam with favourable properties. Increased acceleration potentials are expected to improve the beam characteristics.

References

Abdelaziz Mohamed E 1960 *Extraction of ion beams from the r.f. plasma* MEA-2 Argonne National Lab. USA

Abdelaziz Mohamed E 1962 *IRE Trans. Nucl. Sci.* NS-9 (No. 2) page number 1

Abdelaziz Mohamed E and Elnahas Mohamed A 1969 *Design and construction of a short column* 150-keV *accelerator for neutron generation* UARAEE Int. Rep. 32

Langmuir I and Blodgett K 1923 *Phys. Rev.* **22** 347

Pierce J R 1940 *J. Appl. Phys.* **11** 548

Proceedings of the first international conference on ion sources, Saclay, France 1969. Edited by A. Septier *et al*, published by Imprimerie Louis-Jean, Publication Scientifiques et Literaires